Solvent and Protein Effects on the Structure and Dynamics of the Rhodopsin Chromophore

ARTICLE *in* CHEMPHYSCHEM · SEPTEMBER 2005

Impact Factor: 3.42 · DOI: 10.1002/cphc.200500066 · Source: PubMed

3 AUTHORS:

Ute F Röhrig
Swiss Institute of Bioinformatics
37 PUBLICATIONS **876** CITATIONS
SEE PROFILE

Leonardo Guidoni
Università degli Studi dell'Aquila
89 PUBLICATIONS **1,430** CITATIONS
SEE PROFILE

Ursula Rothlisberger
École Polytechnique Fédérale de Lausanne
291 PUBLICATIONS **8,504** CITATIONS
SEE PROFILE

Solvent and Protein Effects on the Structure and Dynamics of the Rhodopsin Chromophore

Ute F. Röhrig,[a] Leonardo Guidoni,[a] and Ursula Rothlisberger*[a]

*The structure and dynamics of the retinal chromophore of rhodopsin are investigated systematically in different environments (vacuum, methanol solution, and protein binding pocket) and with different computational approaches (classical, quantum, and hybrid quantum mechanics/molecular mechanics (QM/MM) descriptions). Finite temperature effects are taken into account by molecular dynamics simulations. The different components that determine the structure and dynamics of the chromophore in the protein are dissected, both in the dark state and in the early photointermediates. In vacuum and in solution the chromophore displays a very high flexibility, which is significantly reduced by the protein environment. In the 11-*cis *chromophore, the bond-length alternation, which is correlated with the dipole moment, is found to be similar in solution and in the protein, while it differs greatly with respect to minimum-energy vacuum structures. In the model of the earliest protein photointermediate, the highly twisted chromophore shows a very reduced bond-length alternation.*

1. Introduction

Retinal serves as a chromophore in many light-detecting proteins, such as the visual pigment rhodopsin (Rh), the proton pump bacteriorhodopsin, or the phototaxis receptors sensory rhodopsin I and II. In all cases, retinal is covalently bound to the seven-helix transmembrane protein via a protonated or unprotonated Schiff base link with the amino group of a lysine side chain (see Figure 1). Photon absorption triggers a *cis*–*trans* or *trans*–*cis* isomerization of the retinal protonated Schiff base (RPSB), which in turn induces structural changes in the tertiary protein structure and activates ion translocation and/or a signal-transduction pathway.

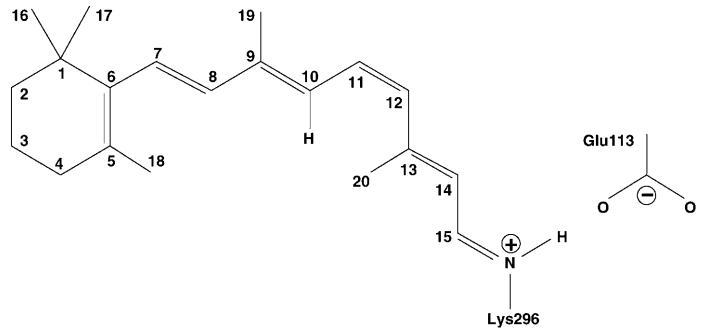

Figure 1. The 11-*cis*-retinal protonated Schiff base in rhodopsin.

The photoreceptor rhodopsin is located in the retina of vertebrates and serves for dim-light vision. The crystal structure of rhodopsin[1–4] provides the first high-resolution structure of the large and pharmaceutically important class of G-protein-coupled receptors[5] and constitutes a major step toward a better understanding of the first steps of the visual cascade. Here, light absorption triggers 11-*cis* to all *trans* isomerization of the RPSB.[6] The primary photoproduct, photorhodopsin, is formed on an ultrafast timescale (200 fs)[7] and with high efficiency (quantum yield 0.65).[8] Photorhodopsin thermally relaxes within a few picoseconds to bathorhodopsin, which still displays a very distorted all-*trans* configuration.[9] Within 40 ns, bathorhodopsin establishes an equilibrium with a blue-shifted intermediate (BSI) before the mixture decays within 200 ns to lumirhodopsin.[10,11] Lumirhodopsin is then transformed into metarhodopsin I and subsequently metarhodopsin II, the active conformation for G-protein coupling.[12]

We have previously investigated the photoreaction in rhodopsin by hybrid quantum/classical (QM/MM)[13] molecular dynamics (MD) simulations of the full protein in a membrane-mimetic environment, and treated the chromophore at the density functional theory (DFT) level.[14] No restraints, either on any structural part of the protein or on the reaction coordinate, were imposed. We have shown that the protein binding pocket selects and accelerates the isomerization exclusively around the C11–C12 bond via preformation of a twisted structure. In $\approx$100 fs, a very twisted all-*trans* chromophore can be formed within the protein binding pocket by minor rearrangement of the nuclei and a clockwise isomerization sense. We were able to show the relaxation of the chromophore on the nanosecond timescale by

[a] *Dr. U. F. Röhrig,[+] Prof. Dr. L. Guidoni,[++] Prof. Dr. U. Rothlisberger*
Laboratory of Computational Chemistry and Biochemistry
Ecole Polytechnique Fédérale de Lausanne (EPFL)
1015 Lausanne (Switzerland)
Fax: (+41) 21-693-0320
E-mail: ursula.roethlisberger@epfl.ch

[+] *Current address:*
E. Fermi Research Center, Dipartimento di Fisica
Università degli studi di Roma "Tor Vergata"
Via della Ricerca Scientifica 1, 00133 Roma (Italy)

[++] *Current address:*
Dipartimento di Fisica, Università degli studi di Roma "La Sapienza"
P. le A. Moro 5, 00185 Roma (Italy)

  DOI: 10.1002/cphc.200500066

classical MD simulations, and to observe changes in the tertiary protein structure that are in agreement with experimental findings.[15]

Herein, we report an investigation of the structure and dynamics of the rhodopsin chromophore. We systematically compare different environments (vacuum, methanol solution, protein binding pocket) and different computational approaches (classical, quantum, QM/MM descriptions), and explicitly include finite temperature effects via molecular dynamics simulations. The goal is to dissect the different components that determine the structure and dynamics of the chromophore in the protein binding pocket, both in the dark state and in the early photointermediates. We will especially focus on 1) the distortion of the chromophore from a planar structure, 2) the bond-length alternation (BLA) and its relationship with the surrounding environment, and 3) the influence of the counterion. These parameters have been previously addressed by theoretical investigations, but mostly by static calculations (geometry optimizations at zero temperature).[16–23] These calculations do not yield information about the dynamical properties of the chromophore, which are especially important in condensed-phase systems with many local minima. On the other hand, the existing molecular dynamics studies either rely solely on empirically parameterized classical force fields,[15,24] or deal only with the chromophore in vacuum.[25–27] To date, only the dark state of rhodopsin has been investigated by hybrid QM/MM MD simulations, which compared different crystal structures.[4]

2. Methods

We applied a QM/MM MD technique[28] based on the Car–Parrinello MD (CPMD)[29] code. The QM subsystem is treated within DFT[30,31] with the BLYP[32,33] functional. We use soft norm-conserving nonlocal Troullier–Martins pseudopotentials[34] and a 70-Ry energy cutoff for the plane-wave expansion of the wave function. The inherent periodicity in the plane-wave calculations is circumvented by solving Poisson's equation for non-periodic boundary conditions,[35] while periodic boundary conditions are retained for the classical simulation box. The wave functions are evolved according to the CPMD scheme,[36,37] with a time step of 4 a.u. ($\approx$0.1 fs) and a fictitious electron mass of 400 a.u. The MM subsystem is described by the AMBER6/parm99[38–40] force field, electrostatic interactions are taken into account by the P3M method,[41] and all bonds involving hydrogen atoms are constrained by the SHAKE[42] algorithm. Steric interactions between the QM and the MM part are modeled by a Lennard–Jones potential as prescribed by the classical force field, whereas electrostatic interactions are taken into account by a Hamiltonian electrostatic coupling scheme.[28,43] All simulations are performed at a temperature of 300 K.

The simulations of the RPSB in methanol solution contain one *N*-ethyl RPSB molecule and one chloride ion solvated in 1619 methanol molecules ($c_{Cl^-} = c_{RPSB} = 15$ mmol L^{-1}). The 1:1 concentration of RPSB and chloride reflects the experimental conditions employed in ref. [44]. The methanol and chloride parameters are taken from the AMBER6/parm99 force field,[39] while the classical parameters for the RPSB were developed using the recommended AMBER procedure. The atomic charges were derived by multiconfigurational RESP fitting,[40,45,46] and the torsional parameters were taken from the work of Tajkhorshid et al. (parameter set B).[47] In addition, improper dihedral potentials were added to all sp^2 carbon atoms to ensure planarity.[48] Classical MD simulations under constant temperature and pressure conditions are carried out for an equilibration phase of 500 ps and a production phase of 4 ns (**MET**$_{class}$) with the AMBER6 program package.[38] During equilibration, the system assumes a constant density of 0.78 g cm^{-3} and an approximately cubic cell size with an edge length of 48 Å. For the QM/MM MD simulations, a cubic quantum cell with an edge length of 18.5 Å is employed, which contains the *N*-ethyl RPSB (57 atoms, charge +1). Two QM/MM simulations (**MET1** and **MET2**) of about 5-ps length (plus 500 fs of equilibration phase) are carried out, by starting from different initial conformations sampled during **MET**$_{class}$.

The rhodopsin simulations are based on a model of the protein in a membrane-mimetic environment that has been shown to be stable without restraints for several nanoseconds.[15] They are based on the crystal structure of bovine rhodopsin (Protein Data Bank accession code 1HZX, chain A).[2] Missing amino acid residues have been added using the loop library of SYBYL (Tripos Inc., St. Louis, MO). The solvent-exposed ionizable groups are in their default ionization state, whereas Asp83 and Glu122 are assumed to be neutral as detected by FTIR experiments.[49] The Schiff base linkage between Lys296 and the RPSB bears a positive charge compensated by the counterion Glu113. Glu181 is also assumed to be charged.[11,15] Overall neutral systems at physiological ion concentration ($\approx$150 mmol L^{-1}) were obtained by adding sodium and chloride ions to the aqueous phase. Heteroatoms included in the crystal structure are not included in the models, except for the RPSB and two palmitic acid residues bound to Cys322 and Cys323. Ten water molecules were placed in the protein core. Their positions were determined by steric and energetic considerations and are in good agreement with the water molecules found in the X-ray structure 1L9H.[3] The cell membrane is mimicked by an approximately 30-Å-wide layer of *n*-octane immersed in a box of water. The protein is immersed in the box using the intracellular part of helix IV as the axis perpendicular to the membrane plane. For the QM/MM calculations, the classical box has a volume of $56\times46\times90$ Å^3 and contains 23 917 atoms, while the classical simulation (**RH**$_{class}$) was carried out with a box of $67\times67\times91$ Å^3 and 39 224 atoms. A total simulation time of 26 ns was carried out for rhodopsin in the dark state (**RH**$_{class}$) with the GROMACS program package.[50,51]

For the QM/MM calculations, a quantum cell with edge lengths of $22.2\times14.7\times14.7$ Å is sufficient to converge the energies and geometries with respect to the cell size. The quantum cell contains the RPSB and the Lys296 side chain up to atom CD (57 atoms, charge +1). Tests were also carried out with the side chain of the counterion Glu113 up to atom CB additionally included in the quantum system (64 atoms, neutral). Where the boundary between the classical and the quantum system cuts through a covalent bond, the quantum

system is saturated by a monovalent pseudopotential.[52] For each system, 500 fs of simulation are carried out for equilibration and 4–5 ps for analysis. Three simulations were carried out. **RH** is a simulation of Rh in the dark-adapted state with the chromophore in its 11-*cis* configuration. The earliest intermediate after photoisomerization (**AT1**, all-*trans* RPSB) is obtained directly from QM/MM excited-state isomerization of the chromophore in situ.[14] Data collection is started after 500 fs of equilibration and is continued for 4.5 ps. The initial structure for the later intermediate **AT2** is obtained from classical MD simulations, where C11–C12 bond isomerization was forced by imposing a harmonic potential on $\phi_{C10-C11-C12-C13}$, which changes its minimum from -10 to $+180°$ in 1.5 ps.[15] Intermediate **AT2** is observed about 2 ns after isomerization and contains a more relaxed RPSB, which is formed by a switch of the ionone ring. All models were relaxed within the QM/MM scheme via simulated annealing[53] of the QM system to obtain reasonable starting structures, prior to MD equilibration at 300 K.

For comparison, 5 ps of CPMD simulations were carried out for the RPSB in vacuum (**VAC**$_{MD}$), by using the same parameters employed for the QM subsystem in the QM/MM calculations and treating the full system on a DFT basis. A few geometry optimizations in vacuum were carried out with the same parameters by employing either the BLYP[32,33] or the PBE[54] functional, which yield very similar geometries. Where included, the chloride ion is also treated on the DFT level.

For comparison and verification, a geometry optimization of the RPSB in vacuum is carried out with the B3LYP[55] functional and the 6-31G** basis set using the Gaussian 03[56] code (**VAC**$_{B3LYP}$). The BLYP and B3LYP torsional potentials around the C11–C12 and C12–C13 bonds are compared by optimizing a planar and a twisted structure ($\phi_{C10-C11-C12-C13}=0$ and 10°, $\phi_{C11-C12-C13-C14}=180$ and $-160°$) and comparing the relative energies.

Dipole moments (μ) for charged systems are calculated with respect to the center of charge. Dynamically generated electrostatic-potential-derived charges (D-RESP charges) are calculated according to the scheme proposed in ref. [43].

Analysis of a large number of trajectories suggests that suitable parameters to monitor some of the characteristic properties mentioned in the introduction are: 1) the dihedral angles along the polyene chain, especially $\phi_{C5-C6-C7-C8}$, $\phi_{C10-C11-C12-C13}$, and $\phi_{C11-C12-C13-C14}$; 2) the twist of the polyene chain (ω_{twist}), defined by the angle between the two planes formed by atoms C6–C7–C8 and C14–C15–N; 4) the BLA, calculated as the sum of all formal single-bond lengths minus the sum of all formal double-bond lengths along the polyene chain between the C6 and N atoms (five single bonds and five double bonds); and 4) the salt bridge distance (d_{salt}), that is, the distance between the Schiff base nitrogen atom and the chloride ion in methanol solution and accordingly the distance between the Schiff base nitrogen atom and the closest oxygen atom of Glu113 in Rh.

3. Results and Discussion

3.1. Optimized Vacuum Geometries of the RPSB

Herein, we are mostly interested in the dynamical finite-temperature structure of the RPSB, but for the sake of comparison we also optimize a few structures in vacuum.

The 11-*cis* (6s-*cis*) RPSB in vacuum (**VAC**$_{cis}$) displays no clear BLA in the polyene chain from C9 to C15, and the formal double bond C13=C14 is longer than the formal single bond C14–C15 (see Figure 2 and Table 1). The structure is almost

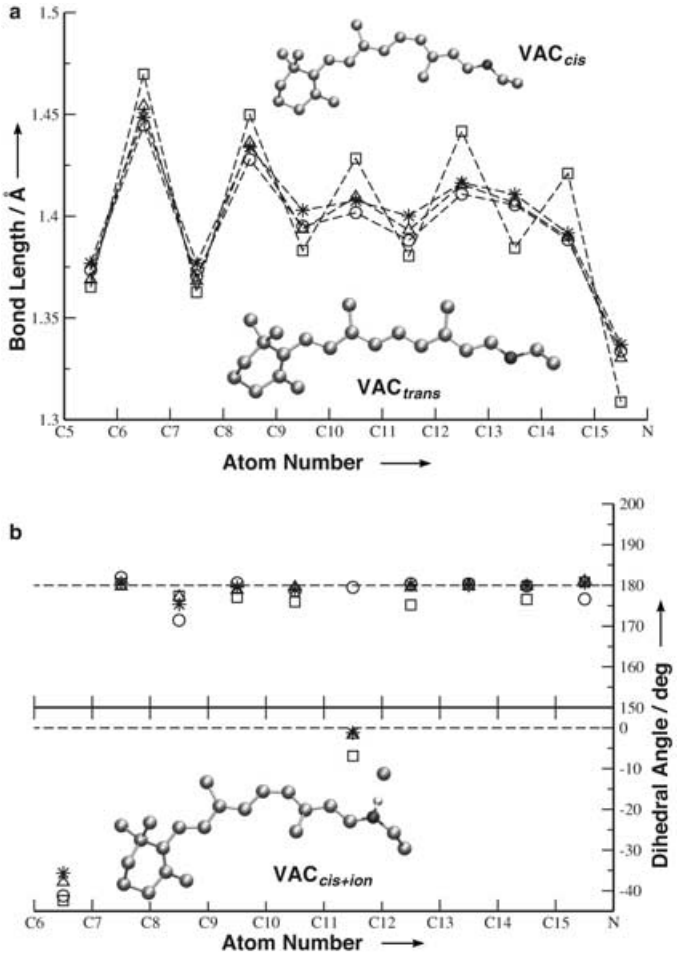

Figure 2. RPSB in vacuo: a) bond lengths and b) dihedral angles for optimized structures (atoms numbered according to Figure 1). **VAC**$_{cis}$ (*), **VAC**$_{B3LYP}$ (△), **VAC**$_{trans}$ (○), **VAC**$_{cis+ion}$ (□).

planar ($\phi_{C10-C11-C12-C13}=-1.2°$, $\omega_{twist}=8.6°$). The smallest bond angles are observed for $\alpha_{C8-C9-C10}$ and $\alpha_{C12-C13-C14}$, around the two methylated carbon atoms, while they are largest for $\alpha_{C10-C11-C12}$ and $\alpha_{C11-C12-C13}$ at the *cis* bond. Starting from an optimized geometry of the RPSB in rhodopsin, we obtained a second vacuum geometry with virtually the same energy ($\Delta E=+0.05$ kcal mol^{-1}), which is more twisted ($\phi_{C10-C11-C12-C13}=-7.9°$, $\omega_{twist}=18.6°$) and displays slightly smaller bond angles and bond lengths. This result suggests 1) that the steric strain

Table 1. Geometrical parameters of the RPSB in vacuum. Distances are given in Å, angles in degrees, and dipole moments in debye. Standard deviations are given in parentheses.

	$\mathbf{VAC}_{cis}$	$\mathbf{VAC}_{B3LYP}$	$\mathbf{VAC}_{trans}$	$\mathbf{VAC}_{cis+ion}$	$\mathbf{VAC}_{MD}$
d_{C5-C6}	1.377	1.369	1.374	1.365	1.38 (0.03)
d_{C6-C7}	1.449	1.454	1.445	1.470	1.46 (0.03)
d_{C7-C8}	1.377	1.368	1.371	1.363	1.38 (0.03)
d_{C8-C9}	1.448	1.436	1.428	1.450	1.44 (0.03)
d_{C9-C10}	1.403	1.394	1.395	1.383	1.41 (0.03)
$d_{C10-C11}$	1.408	1.409	1.402	1.428	1.41 (0.03)
$d_{C11-C12}$	1.400	1.393	1.388	1.381	1.41 (0.03)
$d_{C12-C13}$	1.416	1.416	1.411	1.442	1.42 (0.03)
$d_{C13-C14}$	1.411	1.407	1.406	1.384	1.42 (0.03)
$d_{C14-C15}$	1.392	1.390	1.388	1.421	1.39 (0.03)
d_{C15-N}	1.337	1.330	1.334	1.309	1.35 (0.02)
$\alpha_{C5-C6-C7}$	123.5	123.2	122.9	123.8	124 (3)
$\alpha_{C6-C7-C8}$	129.6	128.8	127.4	128.6	130 (4)
$\alpha_{C7-C8-C9}$	125.5	125.0	125.3	126.0	125 (3)
$\alpha_{C8-C9-C10}$	117.4	117.3	117.1	117.7	117 (3)
$\alpha_{C9-C10-C11}$	126.1	125.5	126.7	126.8	125 (3)
$\alpha_{C10-C11-C12}$	132.1	131.8	123.9	130.6	131 (3)
$\alpha_{C11-C12-C13}$	132.5	131.7	124.9	131.9	132 (3)
$\alpha_{C12-C13-C14}$	117.0	116.8	118.0	116.8	117 (3)
$\alpha_{C13-C14-C15}$	126.7	126.1	125.6	125.6	126 (3)
$\alpha_{C14-C15-N}$	124.5	124.5	124.7	122.5	124 (3)
$\phi_{C5-C6-C7-C8}$	−35.7	−37.8	−41.2	−42.4	−13 (36)
$\phi_{C6-C7-C8-C9}$	180.7	179.8	181.9	180.4	180 (10)
$\phi_{C7-C8-C9-C10}$	175.3	177.2	171.4	177.4	180 (13)
$\phi_{C8-C9-C10-C11}$	179.6	178.9	180.6	177.0	180 (9)
$\phi_{C9-C10-C11-C12}$	178.9	179.5	178.7	176.0	182 (11)
$\phi_{C10-C11-C12-C13}$	−1.2	−1.7	179.5	−6.9	0 (15)
$\phi_{C11-C12-C13-C14}$	180.2	179.6	180.4	175.2	178 (11)
$\phi_{C12-C13-C14-C15}$	180.0	179.8	180.3	180.2	181 (11)
$\phi_{C13-C14-C15-N}$	180.0	179.9	179.8	176.5	179 (9)
$\phi_{C14-C15-N-C}$	180.7	181.0	176.7	180.8	180 (14)
ω_{twist}	6.3	5.9	8.5	19.1	28 (15)
d_{C6-N}	11.7	11.7	12.1	11.5	11.6 (0.2)
d_{salt}	–	–	–	2.92	–
μ	12.6	13.4	13.5	14.8[a]	–

[a] Value calculated for the RPSB only (Cl^- treated classically).

induced by the methyl groups C19 and C20 and by the 11-*cis* bond can be reduced either by twisting dihedral angles or by widening bond lengths and angles, and 2) that the torsional potential around C11–C12 is very soft.

To verify if these findings depend on the employed level of theory, we optimized one structure with the B3LYP functional ($\mathbf{VAC}_{B3LYP}$, see Methods Section). As can be seen in Figure 2 and Table 1, B3LYP yields a slightly lower BLA in the C5 to C8 region and a slightly higher BLA in the C9 to C13 region than BLYP, but the maximum bond-length deviation is only 0.009 Å (C9–C10 bond). $\mathbf{VAC}_{B3LYP}$ is in agreement with earlier B3LYP and MP2 calculations with a smaller basis set (6-31G*).[17] For the protonated Schiff base $C_5H_6NH_2^+$, a model system for the RPSB, it has been shown[57,58] that calculations at the CASPT2, B3LYP, and MP2 levels yield very similar BLAs, while CASSCF calculations[58] overestimate the BLA. The torsional potentials around C11–C12 (B3LYP: 0.16 kcal mol^{-1}; BLYP: 0.17 kcal mol^{-1} for a 10° twist) and around C12–C13 (B3LYP and BLYP: 1.07 kcal mol^{-1} for a 20° twist) are in excellent agreement. In summary, BLYP seems to yield very similar structural features as B3LYP, which has been widely used for the theoretical description of the RPSB.[17,59,60] Therefore, our theoretical approach seems to be well-suited to describe the structure and dynamics of the RPSB in the condensed phase.

An optimized all-*trans* (6s-*cis*) RPSB in vacuo ($\mathbf{VAC}_{trans}$) shows the same bond-length pattern but slightly shorter bonds than the *cis* isomers. The bond angles at C11 and C12 decrease as a result of the sterically less hindered *trans* configuration. The chromophore is twisted in $\phi_{C5-C6-C7-C8}$ (−41°) and in $\phi_{C7-C8-C9-C10}$ (171°), whereas all other dihedral angles are close to planar (see Figure 2). The polyene chain is twisted by 8.6°, which is mostly due to steric interactions with the ionone ring.

The 11-*cis* RPSB was also optimized in vacuo with a chloride counterion ($\mathbf{VAC}_{cis+ion}$) to investigate its structural influence. The anion displays a distance of d_{salt} = 2.92 Å to the Schiff base nitrogen and lies in-line with the N–H bond, which is considerably elongated to 1.12 Å (1.02 Å without the chloride ion). The presence of the counterion changes the overall bond-length pattern, especially in the Schiff base region, where the BLA is recovered. The bond angles and dihedral angles are only slightly affected by the presence of the counterion (see Figure 2 and Table 1).

In conclusion, analysis of the RPSB structures optimized in vacuum suggests that the steric strain introduced in the 11-*cis* conformation through the C20 methyl group can be lowered either by introducing a twist or by increasing bond lengths and bond angles. The presence of a counterion ($\mathbf{VAC}_{cis+ion}$) leaves the overall shape of the chromophore almost unaffected, but drastically alters the bond lengths and the BLA. This crucial effect is often neglected in quantum-chemical cluster calculations on retinal models.

3.2. Car–Parrinello Dynamics of the 11-*cis* RPSB in Vacuum

In the next step, we investigate the dynamics of the 11-*cis* RPSB in vacuum at ambient temperature. We find that in $\mathbf{VAC}_{MD}$ the average bond-length pattern is the same as that in the optimized structures, but the average lengths are 0.005 Å longer than in $\mathbf{VAC}_{cis}$ due to the anharmonicity of the bonding potential. $\phi_{C10-C11-C12-C13}$ is on average 0°, but shows large fluc-

tuations from −38 to +48°, which indicates a large intrinsic flexibility. $\phi_{C5-C6-C7-C8}$ changes during the simulated 5 ps from a negatively twisted conformation (≈−40°) to a positively twisted conformation (≈40°). The average value of all-*trans* dihedral angles is 180±2°, very close to planar. However, ω_{twist} displays an average value of 28±15°, with a maximum at 76° (see Figure 3a), so the whole polyene chain is far from planar and very mobile.

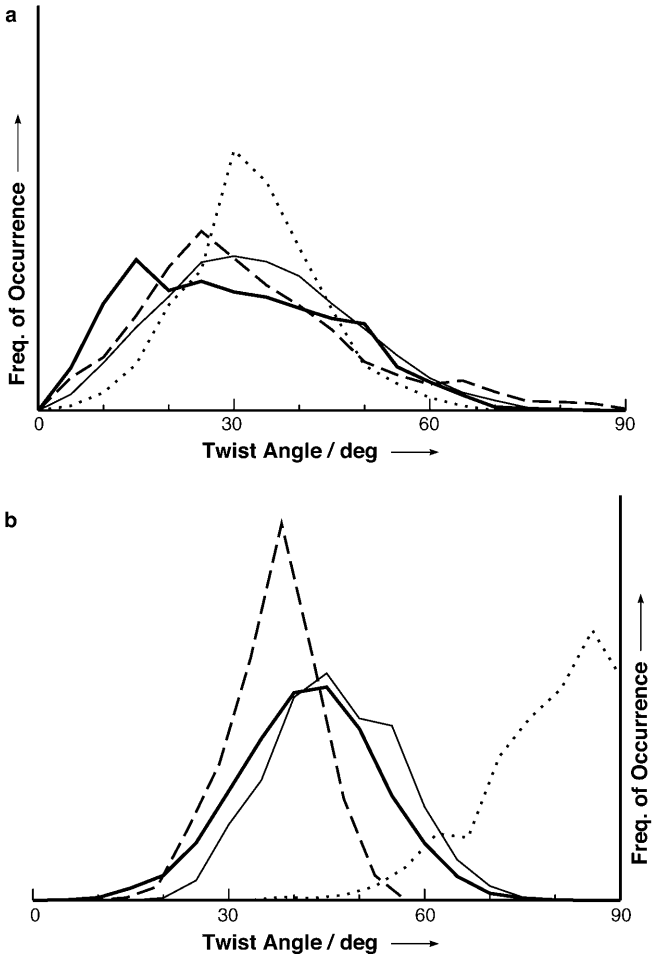

Figure 3. Histograms of the distribution of the twist angle ω_{twist} in different simulations. a) $\mathbf{VAC}_{MD}$ (thick line), $\mathbf{MET}_{class}$ (thin line), **MET1** (•••••), **MET2** (-----). b) $\mathbf{RH}_{class}$ (thick line), **RH** (thin line), **AT1** (•••••), **AT2** (-----).

To show the correlation between geometrical observables and electronic structure, we investigated two snapshots from $\mathbf{VAC}_{MD}$, one with a very high BLA ($\mathbf{VAC}_{MD1}$) and one with a very low BLA ($\mathbf{VAC}_{MD2}$). In $\mathbf{VAC}_{MD1}$, there is a strong BLA throughout the whole polyene chain (see Figure 4a), while in $\mathbf{VAC}_{MD2}$, the conjugation defect, which is usually located in the Schiff base region, has migrated to the ionone ring end. In $\mathbf{VAC}_{MD1}$, the highest occupied molecular orbital (HOMO) is located primarily on the ionone ring, while the lowest unoccupied molecular orbital (LUMO) is located in the Schiff base region, and the molecule has a dipole moment of 15.8 D. In $\mathbf{VAC}_{MD2}$, both orbitals are delocalized over the whole chain, and the corresponding dipole moment is much lower (8.7 D). In the optimized vacuum structure $\mathbf{VAC}_{cis}$, the dipole moment lies between these two values (12.6 D). These large differences in the dipole moment reveal the strong connection between the electronic and the atomic structure. In Figure 4b it can be seen that the conjugation defect migrates a few times to the ionone ring end during the simulated time of 5 ps. Figure 4d shows that the BLA in $\mathbf{VAC}_{MD}$ shows very large fluctuations. During 11% of the time it is even inverted, which means that the sum of the formal double-bond lengths (even including the short C=N bond) is greater than the sum of the formal single-bond lengths. A high mobility of the conjugation defect in the gas phase has been found before, but only for the case of an energetically very unfavorable conformation of the RPSB.[25]

In conclusion, the RPSB shows a remarkable structural flexibility, apparent in the large fluctuations of the torsional angles and ω_{twist}, which can be explored at ambient temperature. This is in contradiction with the common view that the RPSB is rigidly confined to an almost planar structure in vacuum by its conjugated π system. Also, the BLA and the dipole moment show strong fluctuations that even lead to temporary inversions of the single-bond/double-bond pattern in the whole polyene chain.

3.3. Dynamics of the 11-*cis* RPSB in Methanol

3.3.1. Classical MD Simulations

During the equilibration phase of the classical MD simulation in methanol solution ($\mathbf{MET}_{class}$), the chloride ion, which is initially located close to the positively charged protonated Schiff base, diffuses away. However, in the following 4 ns, the chloride ion returns to a distance of 3.5 Å to the Schiff base nitrogen for 70 ps, and another time to a distance of 7 Å for 200 ps, while for the rest of the simulation it moves freely in the solvent. The ionone ring rotates several times around the C6–C7 axis, and shows preferred conformations at a dihedral angle of about −55 and +55°, which correspond to two twisted 6s-*cis* conformations. The 6s-*trans* conformation is only observed transiently (see Figure 5a). Furthermore, there are two equally sampled conformations of the chromophore: one with a positive dihedral angle $\phi_{C10-C11-C12-C13}$ of about +15° and at the same time a negative dihedral angle $\phi_{C11-C12-C13-C14}$ of about −160°, and its mirror image (see Figure 5b). The average retention period in each state is about 50 ps, and the transitions are not correlated with the conformation of $\phi_{C5-C6-C7-C8}$. The remaining dihedral angles of the polyene chain adopt an average value close to 180° (see Table 2) and show no two-state behavior. All bonds in the polyene chain display an average length of 1.41 to 1.42±0.03 Å (force field parameter: 1.40 Å), in agreement with the fact that no BLA has been imposed in the classical model. The ω_{twist} is 31±14°, that is, even larger than in $\mathbf{VAC}_{MD}$. During the simulated time of 4 ns, the twist rises five times to about 90°, so here also the RPSB displays a great flexibility (see Figure 3a).

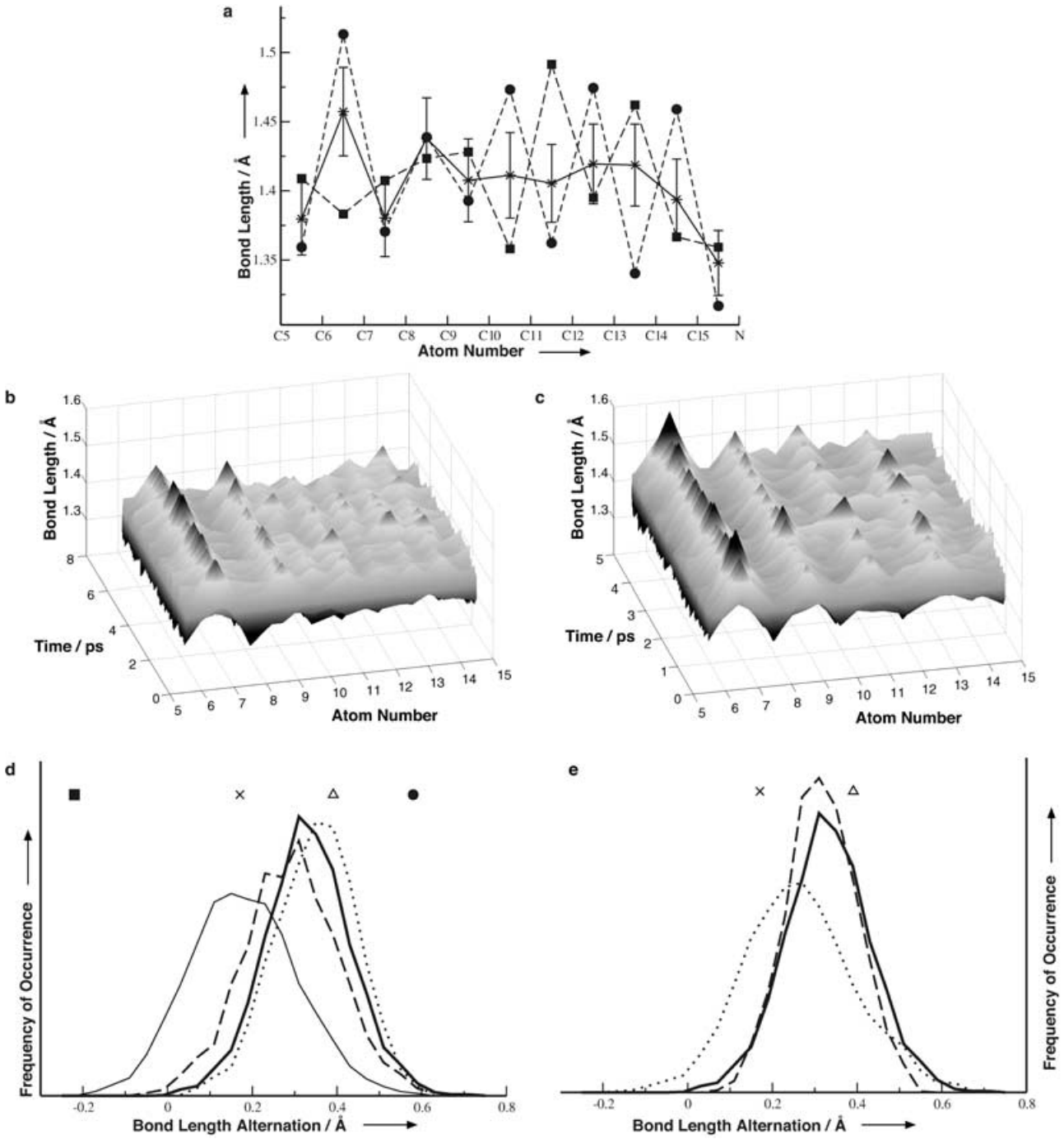

Figure 4. Bond-length alternation of the 11-*cis* RPSB: a) Average from MD simulation in vacuum ($\mathbf{VAC}_{MD}$, *) and two extreme snapshots, one with a very high BLA ($\mathbf{VAC}_{MD1}$, ●), and one with a very low BLA ($\mathbf{VAC}_{MD2}$, ■). b) Bond-length variations in $\mathbf{VAC}_{MD}$. c) Bond-length variations in **RH**. d) Histograms of BLA from $\mathbf{VAC}_{MD}$ (thin line), **RH** (thick line), **MET1** (•••••), and **MET2** (-----). The values for $\mathbf{VAC}_{cis}$ (×), $\mathbf{VAC}_{cis+ion}$ (△), $\mathbf{VAC}_{MD1}$ (●), and $\mathbf{VAC}_{MD2}$ (■) are also given. e) Histogram of BLA from **RH** (thick line), **AT1** (•••••) and **AT2** (-----).

3.3.2. QM/MM MD Simulations

It would be impossible to sample all conformations of the RPSB in methanol on the timescale accessible to an ab initio QM/MM MD simulation, so we chose two representative frames with distinctively different conformations from the classical MD as starting points for two independent QM/MM MD simulations. **MET1** starts from a positive dihedral angle $\phi_{C10-C11-C12-C13}$ and a short salt bridge of 3.25 Å (N–Cl), while **MET2** starts from a negative dihedral angle $\phi_{C10-C11-C12-C13}$, and the chloride ion is not in the vicinity of the RPSB. In **MET1**, the dihedral angle $\phi_{C5-C6-C7-C8}$ fluctuates around −52° (**MET2:** −46°), $\phi_{C10-C11-C12-C13}$ adopts an average value of +9° (**MET2:** −10°), and $\phi_{C11-C12-C13-C14}$ has an average value of −172° (**MET2:** +171°; see Figure 6). No structural transitions are observed during the QM/MM simulations. In **MET2**, ω_{twist} is larger than

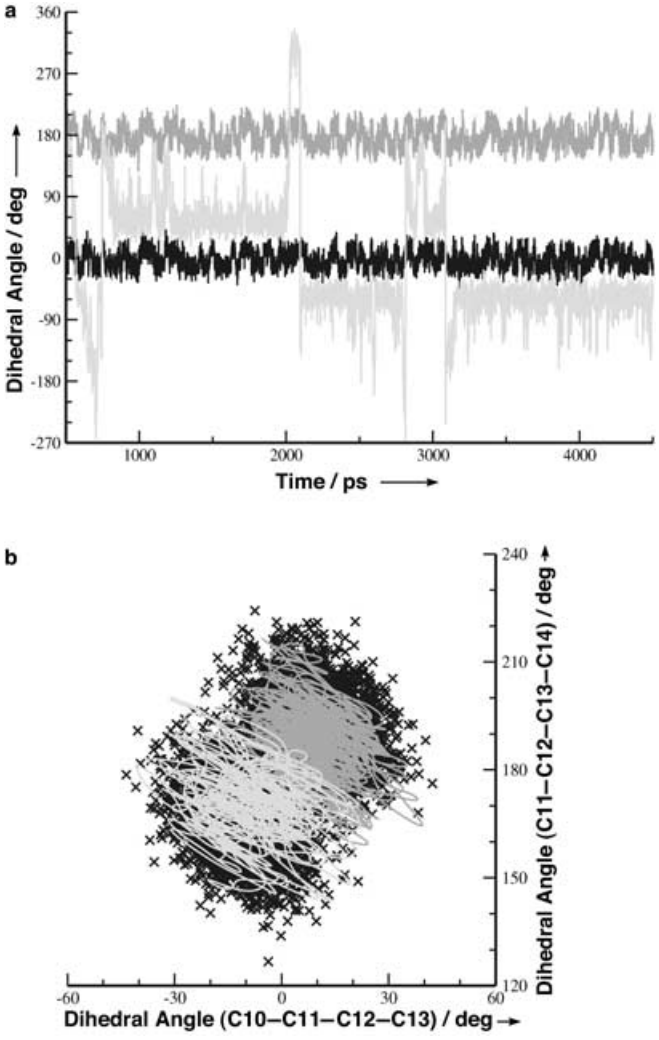

Figure 5. 11-*cis* RPSB in methanol solution. a) Dihedral angles $\phi_{C5-C6-C7-C8}$ (light gray), $\phi_{C10-C11-C12-C13}$ (black) and $\phi_{C11-C12-C13-C14}$ (dark gray) in $\mathbf{MET}_{class}$ b) Correlation between $\phi_{C10-C11-C12-C13}$ and $\phi_{C11-C12-C13-C14}$ in $\mathbf{MET}_{class}$ (black crosses), **MET1** (dark gray), and **MET2** (light gray).

Table 2. Geometrical parameters of the RPSB in methanol. Distances are given in Å, angles in degrees, and dipole moments in debye. Standard deviations are given in parentheses.

	$\mathbf{MET}_{class}$	MET1	MET2
d_{C5-C6}	1.42 (0.03)	1.37 (0.03)	1.37 (0.03)
d_{C6-C7}	1.41 (0.03)	1.48 (0.03)	1.47 (0.04)
d_{C7-C8}	1.41 (0.03)	1.37 (0.02)	1.37 (0.03)
d_{C8-C9}	1.41 (0.03)	1.45 (0.03)	1.45 (0.03)
d_{C9-C10}	1.41 (0.03)	1.39 (0.03)	1.40 (0.03)
$d_{C10-C11}$	1.41 (0.03)	1.43 (0.03)	1.42 (0.03)
$d_{C11-C12}$	1.42 (0.03)	1.39 (0.02)	1.39 (0.03)
$d_{C12-C13}$	1.42 (0.03)	1.44 (0.03)	1.43 (0.03)
$d_{C13-C14}$	1.41 (0.03)	1.40 (0.02)	1.41 (0.03)
$d_{C14-C15}$	1.41 (0.03)	1.41 (0.02)	1.40 (0.03)
d_{C15-N}	1.34 (0.02)	1.32 (0.02)	1.33 (0.02)
$\alpha_{C5-C6-C7}$	121 (3)	123 (3)	123 (3)
$\alpha_{C6-C7-C8}$	122 (3)	127 (4)	127 (4)
$\alpha_{C7-C8-C9}$	124 (3)	127 (3)	127 (3)
$\alpha_{C8-C9-C10}$	117 (3)	117 (3)	117 (3)
$\alpha_{C9-C10-C11}$	124 (3)	125 (3)	125 (3)
$\alpha_{C10-C11-C12}$	126 (3)	131 (3)	131 (4)
$\alpha_{C11-C12-C13}$	129 (3)	132 (3)	133 (3)
$\alpha_{C12-C13-C14}$	115 (3)	115 (3)	115 (3)
$\alpha_{C13-C14-C15}$	124 (3)	127 (3)	127 (3)
$\alpha_{C14-C15-N}$	118 (3)	121 (3)	121 (3)
$\phi_{C5-C6-C7-C8}$	−5 (86)	−52 (14)	−46 (12)
$\phi_{C6-C7-C8-C9}$	180 (8)	183 (9)	179 (10)
$\phi_{C7-C8-C9-C10}$	179 (13)	171 (11)	175 (9)
$\phi_{C8-C9-C10-C11}$	180 (8)	187 (8)	176 (9)
$\phi_{C9-C10-C11-C12}$	179 (10)	180 (11)	178 (10)
$\phi_{C10-C11-C12-C13}$	−2 (14)	9 (10)	−10 (12)
$\phi_{C11-C12-C13-C14}$	178 (16)	188 (10)	171 (10)
$\phi_{C12-C13-C14-C15}$	180 (8)	180 (8)	182 (10)
$\phi_{C13-C14-C15-N}$	180 (8)	182 (8)	177 (11)
$\phi_{C14-C15-N-C}$	180 (9)	182 (9)	182 (11)
ω_{twist}	31 (14)	30 (10)	30 (17)
d_{C6-N}	11.1 (0.3)	11.5 (0.2)	11.5 (0.3)
d_{salt}	17 (7)	3.4 (0.2)	26.6 (0.6)
μ	–	22 (2)	19 (3)

50° for a period of 400 fs, and displays a maximum around 90°. This is not connected with a significant rise in energy and shows that also in a QM description the RPSB can easily adopt a very twisted conformation in solution. The average value of ω_{twist} in both QM/MM simulations compares well to its value in the classical description.

In **MET1**, the salt bridge is maintained throughout the simulation with an average distance of 3.4 ± 0.2 Å between the chloride ion and the Schiff base nitrogen atom (distance N···H = 1.03 ± 0.02 Å). It can be assumed that the stability is due to the limited timescale of the QM/MM simulation, which does not allow crossing of the activation barrier for the ion-pair dissociation. Due to this electrostatic interaction, the positive charge of the chromophore is slightly more localized in the Schiff base end in **MET1** than in **MET2**, as shown by the D-RESP charges (see Figure 7). Also, the BLA in the Schiff base region is more pronounced in **MET1** (see Figures 4d and 6), and the dipole moment is larger (see Table 2). However, due to the large dielectric screening of methanol these effects are relatively small. The counterion effects in the vacuum structure are much larger.

A comparison between the classical force-field description and the QM description of the RPSB in solution shows that the classical model describes the internal degrees of freedom correctly, except for the bond-length pattern, where no alternation is imposed. However, the average length of 1.41 Å is close to the QM value of 1.40 Å, and the overall distance between the C6 and N atoms is even a bit underestimated (11.1 ± 0.3 Å classically versus 11.5 ± 0.3 Å by QM calculations). The dihedral angles sample more space in the classical simulations, but the local minima correspond also to minima in the QM/MM description (see Figure 5b). The twist of the polyene chain is similar in the classical and the QM descriptions, but due to the large fluctuations it only converges on the longer timescale of the classical simulation. In summary, the classical force field for the RPSB yields an excellent description of the structural and dynamical properties.

A comparison between the QM dynamics of the 11-*cis* RPSB in vacuum and in methanol solution yields significant differences between these environments. The BLA in methanol is much higher than in the vacuum dynamics due to the influen-

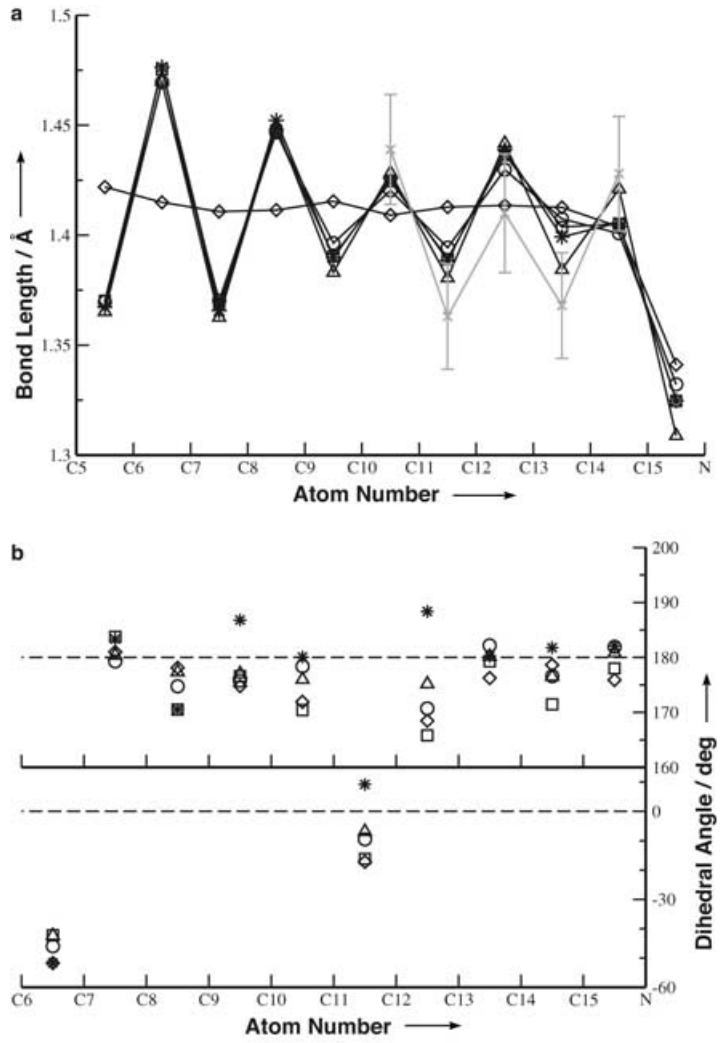

Figure 6. a) Bond lengths and b) dihedral angles of the 11-*cis* RPSB in methanol solution and in Rh; **MET1** (*), **MET2** (○), **RH** (□), $\mathbf{RH}_{class}$ (◇). $\mathbf{VAC}_{cis+ion}$ (△) and the bond lengths determined by NMR in ref. [63] (gray) are given for comparison.

ces of the counterion and the polar solvent (see Figure 4d), but is not comparable to $\mathbf{VAC}_{cis+ion}$. Interestingly, the solvent induces a two-state behavior concerning the conformation around $\phi_{C10-C11-C12-C13}$ and $\phi_{C11-C12-C13-C14}$. Both torsional angles display one conformation with a positive twist and one with a negative twist. In addition, these two conformations become coupled: $\phi_{C11-C12-C13-C14}$ is positive when $\phi_{C10-C11-C12-C13}$ is negative, and vice versa (see Figure 5a). These two stereoisomers minimize the steric repulsion between the C20 methyl group and the hydrogen atom at C10. In contrast, in the gas phase these two dihedral angles fluctuate independently around a planar average structure. Solvation therefore favors the twisted minima, probably due to a more favorable solvation free energy.

In summary, classical and hybrid QM/MM MD simulations of the 11-*cis* RPSB in methanol solution show that within the employed methodology: 1) only the 6s-*cis* conformation is stable; 2) the BLA is in between the values of the vacuum structures without and with a counterion; 3) the methanol solution stabilizes twisted conformations of the chromophore; 4) the motion of $\phi_{C10-C11-C12-C13}$ and $\phi_{C11-C12-C13-C14}$ becomes correlated in solution; 5) the RPSB is very flexible also in solution; and 6) a good agreement between MM and QM/MM simulations is observed.

3.4. Dynamics of the 11-*cis* RPSB in Rhodopsin

3.4.1. Classical MD Simulations

In contrast to the situation in vacuum and in methanol solution, it has been shown that in the rhodopsin binding pocket the RPSB adopts one unique conformation, and no transition is observed within several nanoseconds of classical MD simulation.[15,24] These results have been corroborated by quantum chemical and QM/MM calculations.[18,19,61] The conformation of the β-ionone ring in the crystal structure of rhodopsin is 6s-*cis* with a negative twist angle. In the protein binding pocket as resolved by the X-ray data,[1,2] only the conformer with a positive helicity around the C12–C13 bond can be accommodated due to steric constraints.[15,18,24]

Here, a classical MD simulation of rhodopsin in the dark state ($\mathbf{RH}_{class}$) is carried out for the sake of comparison with the QM/MM results. We use the same force field for the description of the RPSB as in methanol solution, so the BLA is not captured in the classical model (see Figure 6a). The average C–C bond length is again 1.41 ± 0.03 Å, but the overall length of the polyene chain is slightly shorter (11.0 ± 0.2 Å versus 11.1 ± 0.3 Å in methanol, see Table 3), which indicates that the molecule is a little more bent. As observed before, the dihedral angles are all stable in

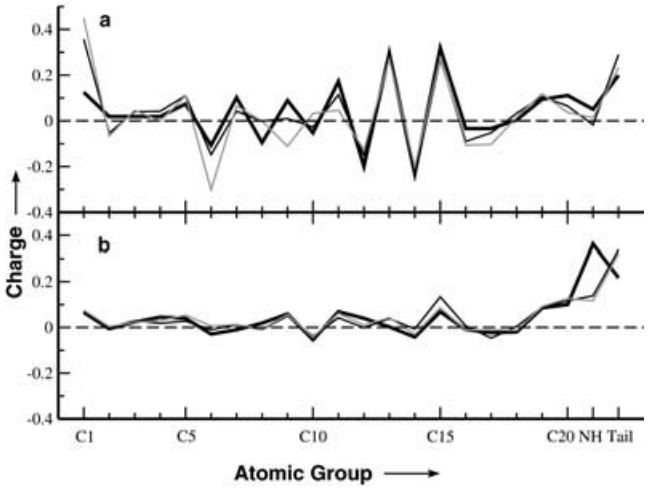

Figure 7. Comparison of classical point charges with DFT/ESP charges. a) ESP charges of the 11-*cis* RPSB in vacuum. The ESP charges of the optimized geometries $\mathbf{VAC}_{cis}$ (thin line) and $\mathbf{VAC}_{cis+ion}$ (gray line, the charge of −0.7 on the chloride atom not shown) are compared to the charges used in the classical model (thick line). b) D-RESP charges[43] obtained in **MET1** (thin line), **MET2** (gray line), and **RH** (thick line).

Table 3. Geometrical parameters of the RPSB in rhodopsin. Distances are given in Å, angles in degrees, and dipole moments in debye. Standard deviations are given in parentheses.

	RH_{class}	RH	AT1	AT2
d_{C5-C6}	1.42 (0.02)	1.37 (0.03)	1.37 (0.03)	1.37 (0.02)
d_{C6-C7}	1.41 (0.03)	1.48 (0.03)	1.47 (0.04)	1.46 (0.03)
d_{C7-C8}	1.41 (0.03)	1.37 (0.03)	1.38 (0.03)	1.37 (0.02)
d_{C8-C9}	1.41 (0.03)	1.45 (0.03)	1.44 (0.04)	1.44 (0.02)
d_{C9-C10}	1.42 (0.03)	1.39 (0.03)	1.40 (0.03)	1.39 (0.02)
$d_{C10-C11}$	1.41 (0.03)	1.42 (0.03)	1.42 (0.03)	1.42 (0.02)
$d_{C11-C12}$	1.41 (0.03)	1.39 (0.03)	1.39 (0.03)	1.38 (0.02)
$d_{C12-C13}$	1.41 (0.03)	1.44 (0.03)	1.43 (0.03)	1.43 (0.02)
$d_{C13-C14}$	1.41 (0.03)	1.40 (0.02)	1.41 (0.03)	1.40 (0.02)
$d_{C14-C15}$	1.40 (0.03)	1.41 (0.03)	1.40 (0.03)	1.41 (0.02)
d_{C15-N}	1.34 (0.03)	1.32 (0.02)	1.33 (0.02)	1.31 (0.02)
$\alpha_{C5-C6-C7}$	122 (3)	123 (3)	125 (3)	124 (3)
$\alpha_{C6-C7-C8}$	121 (3)	127 (4)	129 (4)	130 (4)
$\alpha_{C7-C8-C9}$	125 (3)	127 (3)	126 (4)	126 (3)
$\alpha_{C8-C9-C10}$	116 (3)	117 (3)	116 (3)	118 (3)
$\alpha_{C9-C10-C11}$	124 (3)	125 (3)	125 (4)	125 (3)
$\alpha_{C10-C11-C12}$	125 (3)	131 (3)	124 (4)	125 (3)
$\alpha_{C11-C12-C13}$	130 (3)	132 (3)	126 (4)	125 (2)
$\alpha_{C12-C13-C14}$	115 (3)	115 (3)	119 (3)	119 (3)
$\alpha_{C13-C14-C15}$	124 (3)	127 (3)	124 (3)	123 (3)
$\alpha_{C14-C15-N}$	119 (3)	121 (3)	123 (3)	125 (3)
$\phi_{C5-C6-C7-C8}$	−52 (10)	−42 (10)	−21 (15)	−18 (15)
$\phi_{C6-C7-C8-C9}$	181 (8)	184 (8)	205 (9)	193 (8)
$\phi_{C7-C8-C9-C10}$	178 (10)	171 (9)	163 (11)	174 (9)
$\phi_{C8-C9-C10-C11}$	175 (7)	177 (7)	219 (8)	193 (8)
$\phi_{C9-C10-C11-C12}$	172 (8)	170 (9)	173 (7)	175 (8)
$\phi_{C10-C11-C12-C13}$	−17 (8)	−16 (11)	212 (8)	190 (8)
$\phi_{C11-C12-C13-C14}$	168 (7)	166 (8)	186 (8)	178 (8)
$\phi_{C12-C13-C14-C15}$	176 (7)	179 (7)	194 (9)	185 (8)
$\phi_{C13-C14-C15-N}$	179 (7)	171 (8)	179 (9)	167 (8)
$\phi_{C14-C15-N-C}$	176 (7)	178 (7)	186 (8)	184 (9)
ω_{twist}	40 (11)	44 (10)	79 (12)	35 (7)
d_{C6-N}	11.0 (0.2)	11.2 (0.1)	11.3 (0.2)	12.0 (0.1)
d_{salt}	2.7 (0.1)	2.7 (0.1)	2.7 (0.1)	2.8 (0.1)
μ	–	21 (1)	18 (2)	24 (2)

one state, and no transition is observed during 26 ns of simulated time. The dihedral angle $\phi_{C5-C6-C7-C8}$ assumes a value of $-52\pm10°$, which corresponds to one of the minima in $\mathbf{MET}_{class}$ $\phi_{C10-C11-C12-C13}$ ($-17\pm8°$), $\phi_{C11-C12-C13-C14}$ ($168\pm7°$), and ω_{twist} ($40\pm11°$) are about 10 to 15° more twisted than in $\mathbf{MET}_{class}$, but the averages lie within the standard deviation of the solution values (see Tables 2 and 3). This means that the protein stabilizes a slightly more bent conformation of the RPSB, as does the methanol solution.

3.4.2. QM/MM MD Calculations

Apart from the BLA, the use of a QM description of the chromophore yields again surprisingly similar results to the classical force-field description. The dihedral angle $\phi_{C5-C6-C7-C8}$ ($-42\pm10°$) is ten degrees smaller than in $\mathbf{RH}_{class}$, while the dihedral angles found in the C9 to C14 region, so around the 11-*cis* bond, agree very well with the classical description (see Figure 6). The ω_{twist} amounts to $44\pm10°$, close to the classical value. The salt bridge between the Schiff base nitrogen atom (QM) and the closer carboxyl oxygen atom of Glu113 has a value of 2.7 ± 0.1 Å, in excellent agreement with the purely classical distance. Shorter QM/MM MD simulations have also been carried out with both the chromophore and the side chain of Glu113 treated on the QM level. No significant differences can be detected, and most importantly the Schiff base proton is never exchanged, in agreement with the observation of a very high pK_a of the RPSB in rhodopsin.[62]

Comparison between the QM/MM structure and dynamics of the RPSB in methanol solution and in rhodopsin reveals some important similarities and differences. The average bond lengths are very similar, more precisely the **RH** values are in between the values found in **MET1** and **MET2** (see Figure 6), while they show less BLA than the vacuum structure with the counterion (see Figure 4d). In comparison to the gas-phase simulation without counterion ($\mathbf{VAC}_{MD}$), the average BLA is higher, and the conjugation defect is localized in the Schiff base moiety of the chain (see Figure 4c). The bond lengths from C10 to C15 observed in our simulations are within or very close to the error margins of the bond lengths deduced from recent solid-state NMR experiments of the chromophore in rhodopsin,[63] except for the C13–C14 bond which is longer in our simulations (1.404 ± 0.025 versus 1.368 ± 0.024 Å, see Figure 6a). However, it must be noted that the NMR values are in even better agreement with the bond lengths of $\mathbf{VAC}_{cis+ion}$. Nevertheless, the conclusion of the authors, that the protein environment does not fix the positive charge on the nitrogen atom as strongly as a counterion in a molecular crystal, agrees with our observations (comparing the BLA of $\mathbf{VAC}_{cis+ion}$ and **RH**). In summary, the BLA suggests that the protein provides a dielectric environment similar to that of methanol, while the fine-tuning is provided by the distance of the counterion. Our results are possibly in disagreement with Raman spectra of the RPSB in methanol solution (ethylenic stretching frequency $1562\,cm^{-1}$) and in rhodopsin ($1546\,cm^{-1}$),[64] which suggest a higher BLA in solution. The discrepancy could be due to the classical methanol model or to insufficient sampling and is subject to further investigations.

As regards the dihedral angles, **RH** is most similar to **MET2**, but **RH** is generally a bit more twisted. However, it is clear that a similar conformation is a local minimum in solution. The ω_{twist} is $44\pm10°$, about 14° larger than the average value in so-

lution (see Figure 3). The dipole moment is of the same order of magnitude in **RH** (20.5 ± 1.4 D) as in methanol solution, but it shows smaller fluctuations, which might be related to the smaller structural fluctuations.

To extend our comparison of the classical versus the QM/MM results to the electrostatic properties, we analyze the atomic charges. In Figure 7 we compare the charges derived by the recommended AMBER procedure[40] with the atomic charges obtained from DFT calculations in vacuum and in the condensed phase. In the case of the classical charges, the 11-*cis* and the all-*trans* RPSB were optimized in the gas phase on the HF/6-31G* level; a restrained ESP (RESP) fitting scheme was used.[40] As is evident from Figure 7, these charges agree well with the vacuum DFT/ESP charges, except for the buried C1 atom. Surprisingly, these charges also remain almost the same in the presence of the chloride ion (**VAC**$_{cis+\text{ion}}$), except for somewhat more negative charges on the C6, C9, and C11 atoms. However, the D-RESP charges calculated as an average over about 5 ps of MD simulations in rhodopsin (**RH**) are quite different. Along the polyene chain charges are close to zero, and only on the C15 atom, the NH group, and the aliphatic tail is an accumulation of positive charge observed. In **MET1** and **MET2**, the positive charge is less localized on the NH group but more localized on the tail. In summary, the atomic charges used in the classical force field do not closely resemble those calculated from the QM/MM scheme, but as shown above this does not significantly alter the structure and dynamics of the RPSB.

In conclusion, simulations of the 11-*cis* RPSB in rhodopsin show that: 1) the protonation state of the chromophore is stable; 2) the protein environment stabilizes a slightly more twisted structure than the solvent; 3) the protein restricts the accessible conformational space of the RPSB drastically; and 4) the electronic structure of the RPSB in the protein, as reflected in the BLA, is similar to the solution structure.

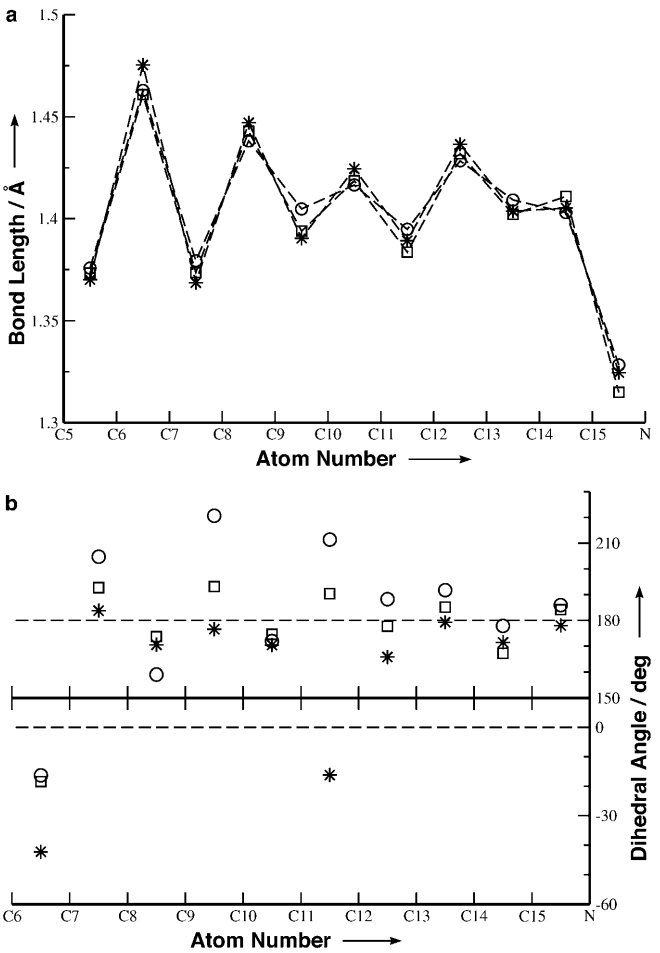

Figure 8. a) Bond lengths and b) dihedral angles of the all-*trans* RPSB in Rh; **AT1** (○), **AT2** (□). For comparison the values of **RH** (*) are also given.

3.5. QM/MM Dynamics of the All-*trans* RPSB in Rhodopsin

Classical and hybrid QM/MM MD simulations have provided some insight into the mechanism of the primary reaction in rhodopsin and into the subsequent steps in the intramolecular signal-transduction pathway.[4, 14, 15, 21, 24] Here, we use structural information from our earlier studies as an input for QM/MM MD simulations. **AT1** features a highly twisted and bent chromophore that is formed approximately 200 fs after the ultrafast photoisomerization (see Methods Section). The relaxation of the internal degrees of freedom from **AT1** to **AT2** takes place on the nanosecond timescale. In **AT1** the RPSB has not moved much from its dark-state position and no large-scale structural changes take place, while in **AT2** the chromophore moves closer to the extracellular loop E2, and away from helices V and VI. We have discussed the changes in the protein structure in more detail in ref. [15].

In **AT1** the BLA is much less pronounced than in **RH** (see Figure 4e), in fact it resembles the gas-phase dynamics of the RPSB without any counterion (Figure 4d). The internal stress in **AT1** can clearly be seen from the deviation of the dihedral angles from a planar all-*trans* structure (see Figure 8b) and from ω_{twist} (79 ± 12°, see Table 3 and Figure 3). The salt bridge between the RPSB and the counterion Glu113 is preserved, and the bulky ionone ring does not change its position during the timescale of the QM/MM simulation. It is interesting to note that steric strain and the subsequent relaxation seem to be located mostly in the C6 to C12 moiety of the chromophore, while the C12 to N moiety remains almost unaltered. In addition, mostly the dihedral angles around the double bonds are affected (see Figure 8b).

The observed "ring flip" between **AT1** and **AT2**[15] is not due to a change in the dihedral angle $\phi_{\text{C5–C6–C7–C8}}$, but rather to a concerted relaxation of the dihedral angles in the polyene chain (see Table 3). Due to this relaxation, ω_{twist} drops from 79° in **AT1** to below its dark-state value in **AT2** (see Figure 3), and the observed BLA is similar to that found in the dark state. The total elongation of the polyene chain approaches its optimal gas-phase value.

In both simulations, the salt bridge between the protonated Schiff base and Glu113 is preserved. The dipole moment increases from **AT1** to **AT2** (see Table 3), which reflects the elongation of the chromophore during the relaxation.

In summary, the simulations of the models of the early photointermediates show that: 1) while the BLA is substantially decreased in **AT1**, it relaxes back to the dark state distribution in **AT2**; 2) ω_{twist} is very large in **AT1** and much lower in **AT2**; and 3) the salt bridge remains stable. These findings are in agreement with the experimental detection of a twisted structure in bathorhodopsin, which is relaxed in the later photointermediates.[9]

4. Conclusions

Our simulations reveal new insights into the structure and dynamics of the retinal protonated Schiff base in different environments. In the isolated chromophore, the steric strain introduced in the 11-*cis* conformation by the C20 methyl group can be lowered either by introducing a twist or by increasing bond lengths and bond angles. The presence of a counterion leaves the overall shape of the chromophore almost unaffected, but drastically increases the BLA.

Vacuum MD studies of the RPSB without counterion show that the chromophore is very flexible and can easily adopt very twisted geometries at ambient temperature. The BLA is weak and for about 10% of the time even inverted. The BLA pattern is correlated with the dipole moment of the RPSB: the stronger the BLA, the more the HOMO is localized in the ionone ring region, and the higher is the dipole moment.

Simulations of the 11-*cis* RPSB in methanol solution show that only the 6*s*-*cis* conformation is stable, the BLA is in between the values of the vacuum structures without and with a counterion, the methanol solution stabilizes twisted conformations of the chromophore, the motions of $\phi_{C10-C11-C12-C13}$ and $\phi_{C11-C12-C13-C14}$ become correlated in solution, the RPSB is very flexible, and the agreement between MM and QM/MM simulations is generally excellent.

MD simulations of the 11-*cis* RPSB in rhodopsin demonstrate that the electronic structure of the RPSB in the protein, as reflected in the BLA, is similar to that in solution. The atomic charges used in the classical force field of the RPSB do not closely resemble those calculated from the QM/MM scheme, but this does not significantly alter its structure and dynamics. The protein environment stabilizes a slightly more twisted structure than the solvent, while its main effect is to restrict the accessible conformational space of the RPSB.

Finally, the simulations of the models of the early photointermediates show that in the earliest intermediate, both the BLA and the twist in the polyene chain are drastically altered, whereas they are substantially relaxed in the later intermediate. On the basis of our results, we propose to call the early all-*trans* structure (**AT1**) "highly twisted," but not the dark-state structure of the RPSB in rhodopsin, as is often the case.[4, 18, 61, 65–67]

Acknowledgements

L.G. acknowledges funding from the VELUX foundation. Computational resources have been granted by CINECA (MINOS Project Number 01/438-7) and the Swiss Center for Scientific Computing (CSCS).

Keywords: chromophores · density functional calculations · isomerization · molecular dynamics · rhodopsin

[1] K. Palczewski, T. Kumasaka, T. Hori, C. A. Behnke, H. Motoshima, B. A. Fox, I. Le Trong, D. C. Teller, T. Okada, R. E. Stenkamp, M. Yamamoto, M. Miyano, *Science* **2000**, *289*, 739 – 745.
[2] D. C. Teller, T. Okada, C. A. Behnke, K. Palczewski, R. E. Stenkamp, *Biochemistry* **2001**, *40*, 7761 – 7772.
[3] T. Okada, Y. Fujiyoshi, M. Silow, J. Navarro, E. M. Landau, Y. Shichida, *Proc. Natl. Acad. Sci. USA* **2002**, *99*, 5982 – 5987.
[4] T. Okada, M. Sugihara, A.-N. Bondar, M. Elstner, P. Entel, V. Buss, *J. Mol. Biol.* **2004**, *342*, 571 – 583.
[5] D. R. Flower, *Biochim. Biophys. Acta* **1999**, *1422*, 207 – 234.
[6] T. Yoshizawa, G. Wald, *Nature* **1963**, *197*, 1279 – 1285.
[7] R. W. Schoenlein, L. A. Peteanu, R. A. Mathies, C. V. Shank, *Science* **1991**, *254*, 412 – 415.
[8] J. E. Kim, M. J. Taubner, R. A. Mathies, *Biochemistry* **2001**, *40*, 13774 – 13778.
[9] I. Palings, E. M. van den Berg, J. Lugtenburg, R. A. Mathies, *Biochemistry* **1989**, *28*, 1498 – 1507.
[10] S. J. Hug, J. W. Lewis, D. S. Kliger, *Biochemistry* **1990**, *29*, 1475 – 1485.
[11] J. W. Lewis, I. Szundi, M. A. Kazmi, T. P. Sakmar, D. S. Kliger, *Biochemistry* **2004**, *43*, 12614 – 12621.
[12] D. S. Kliger, J. W. Lewis, *Isr. J. Chem.* **1995**, *35*, 289 – 307.
[13] A. Warshel, M. Levitt, *J. Mol. Biol.* **1976**, *103*, 227 – 249.
[14] U. F. Röhrig, L. Guidoni, A. Laio, I. Frank, U. Rothlisberger, *J. Am. Chem. Soc.* **2004**, *126*, 15328 – 15329.
[15] U. F. Röhrig, L. Guidoni, U. Rothlisberger, *Biochemistry* **2002**, *41*, 10799 – 10809.
[16] F. Buda, P. Giannozzi, F. Mauri, *J. Phys. Chem. B* **2000**, *104*, 9048 – 9053.
[17] H. M. Lee, J. Kim, C.-J. Kim, K. S. Kim, *J. Chem. Phys.* **2002**, *116*, 6549 – 6559.
[18] M. Sugihara, V. Buss, P. Entel, M. Elstner, T. Frauenheim, *Biochemistry* **2002**, *41*, 15259 – 15266.
[19] N. Ferré, M. Olivucci, *J. Am. Chem. Soc.* **2003**, *125*, 6868 – 6869.
[20] M. Schreiber, V. Buss, M. Sugihara, *J. Chem. Phys.* **2003**, *119*, 12045 – 12048.
[21] J. A. Gascon, V. S. Batista, *Biophys. J.* **2004**, *87*, 2931 – 2941.
[22] S. I. E. Touw, H. J. M. de Groot, F. Buda, *J. Phys. Chem. B* **2004**, *108*, 13560 – 13572.
[23] T. Andruniow, N. Ferre, M. Olivucci, *Proc. Natl. Acad. Sci. USA* **2004**, *101*, 17908 – 17913.
[24] J. Saam, E. Tajkhorshid, S. Hayashi, K. Schulten, *Biophys. J.* **2002**, *83*, 3097 – 3112.
[25] F. Buda, H. J. M. de Groot, A. Bifone, *Phys. Rev. Lett.* **1996**, *77*, 4474 – 4477.
[26] A. Bifone, H. J. M. de Groot, F. Buda, *J. Phys. Chem. B* **1997**, *101*, 2954 – 2958.
[27] C. Molteni, I. Frank, M. Parrinello, *J. Am. Chem. Soc.* **1999**, *121*, 12177 – 12183.
[28] A. Laio, J. VandeVondele, U. Rothlisberger, *J. Chem. Phys.* **2002**, *116*, 6941 – 6947.
[29] CPMD V3.8 Copyright IBM Corp **1990**–**2001**, Copyright MPI fuer Festkoerperforschung Stuttgart **1997**–**2001**. http://www.cpmd.org.
[30] P. Hohenberg, W. Kohn, *Phys. Rev. B* **1964**, *136*, 864 – 871.
[31] W. Kohn, L. J. Sham, *Phys. Rev. A* **1965**, *140*, 1133 – 1138.
[32] A. D. Becke, *Phys. Rev. A* **1988**, *38*, 3098 – 3100.
[33] C. Lee, W. Yang, R. G. Parr, *Phys. Rev. B* **1988**, *37*, 785 – 789.
[34] N. Troullier, J. L. Martins, *Phys. Rev. B* **1991**, *43*, 1993 – 2006.
[35] R. W. Hockney, *Methods Comput. Phys.* **1970**, *9*, 135 – 211.
[36] R. Car, M. Parrinello, *Phys. Rev. Lett.* **1985**, *55*, 2471 – 2474.
[37] D. Marx, J. Hutter. Ab initio molecular dynamics: theory and implementation. In *Modern Methods and Algorithms of Quantum Chemistry* (Ed.: J. Grotendorst), vol. 1 of *NIC Series*, Forschungszentrum Jülich, **2000**, pp. 301 – 449.

[38] AMBER6, D. A. Case, D. A. Pearlman, J. W. Caldwell, T. E. Cheatham III, W. S. Ross, C. L. Simmerling, T. A. Darden, K. M. Merz, R. V. Stanton, A. L. Cheng, J. J. Vincent, M. Crowley, V. Tsui, R. J. Radmer, Y. Duan, J. Pitera, I. Massova, G. L. Seibel, U. C. Singh, P. K. Weiner, P. A. Kollman. University of California, San Francisco, **1999**.
[39] W. D. Cornell, P. Cieplak, C. I. Bayly, I. R. Gould, K. M. Merz, Jr., D. M. Ferguson, D. C. Spellmeyer, T. Fox, J. W. Caldwell, P. A. Kollman, *J. Am. Chem. Soc.* **1995**, *117*, 5179 – 5197.
[40] J. Wang, P. Cieplak, P. A. Kollman, *J. Comput. Chem.* **2000**, *21*, 1049 – 1074.
[41] P. H. Huenenberger, *J. Chem. Phys.* **2000**, *113*, 10464 – 10476.
[42] W. F. van Gunsteren, H. Berendsen, *Mol. Phys.* **1977**, *34*, 1311 – 1327.
[43] A. Laio, J. VandeVondele, U. Rothlisberger, *J. Phys. Chem. B* **2002**, *106*, 7300 – 7307.
[44] P. E. Blatz, J. H. Mohler, H. V. Navangul, *Biochemistry* **1972**, *11*, 848 – 855.
[45] C. I. Bayly, P. Cieplak, W. D. Cornell, P. A. Kollman, *J. Phys. Chem.* **1993**, *97*, 10269 – 10280.
[46] W. D. Cornell, P. Cieplak, C. I. Bayly, P. A. Kollman, *J. Am. Chem. Soc.* **1993**, *115*, 9620 – 9631.
[47] E. Tajkhorshid, J. Baudry, K. Schulten, S. Suhai, *Biophys. J.* **2000**, *78*, 683 – 693.
[48] The employed force field is a slightly modified version of the force field employed in ref. [15].
[49] K. Fahmy, F. Jaeger, M. Beck, T. A. Zvyaga, T. P. Sakmar, F. Siebert, *Proc. Natl. Acad. Sci. USA* **1993**, *90*, 10206 – 10210.
[50] E. Lindahl, B. Hess, D. van der Spoe, *J. Mol. Model.* **2001**, *7*, 306 – 317.
[51] H. J. C. Berendsen, D. van der Spoel, R. van Drunen, *Comput. Phys. Commun.* **1995**, *91*, 43 – 56.
[52] O. A. von Lilienfeld, I. Tavernelli, U. Rothlisberger, D. Sebastiani, *J. Chem. Phys.* **2005**, *122*, 14113.
[53] S. Kirkpatrick, C. D. Gelatt, Jr., M. P. Vecchi, *Science* **1983**, *220*, 671 – 680.
[54] J. P. Perdew, K. Burke, M. Ernzerhof, *Phys. Rev. Lett.* **1996**, *77*, 3865 – 3868.
[55] A. D. Becke, *J. Chem. Phys.* **1993**, *98*, 5648 – 5652.
[56] Gaussian 03, M. J. Frisch, G. W. Trucks, H. B. Schlegel, G. E. Scuseria, M. A. Robb, J. R. Cheeseman, J. A. Montgomery, Jr., T. Vreven, K. N. Kudin, J. C. Burant, J. M. Millam, S. S. Iyengar, J. Tomasi, V. Barone, B. Mennucci, M. Cossi, G. Scalmani, N. Rega, G. A. Petersson, H. Nakatsuji, M. Hada, M. Ehara, K. Toyota, R. Fukuda, J. Hasegawa, M. Ishida, T. Nakajima, Y. Honda, O. Kitao, H. Nakai, M. Klene, X. Li, J. E. Knox, H. P. Hratchian, J. B. Cross, C. Adamo, J. Jaramillo, R. Gomperts, R. E. Stratmann, O. Yazyev, A. J. Austin, R. Cammi, C. Pomelli, J. W. Ochterski, P. Y. Ayala, K. Morokuma, G. A. Voth, P. Salvador, J. J. Dannenberg, V. G. Zakrzewski, S. Dapprich, A. D. Daniels, M. C. Strain, O. Farkas, D. K. Malick, A. D. Rabuck, K. Raghavachari, J. B. Foresman, J. V. Ortiz, Q. Cui, A. G. Baboul, S. Clifford, J. Cioslowski, B. B. Stefanov, G. Liu, A. Liashenko, P. Piskorz, I. Komaromi, R. L. Martin, D. J. Fox, T. Keith, M. A. Al-Laham, C. Y. Peng, A. Nanayakkara, M. Challacombe, P. M. W. Gill, B. Johnson, W. Chen, M. W. Wong, C. Gonzalez, J. A. Pople, Gaussian, Inc., Pittsburgh, PA, **2003**.
[57] C. S. Page, M. Olivucci, *J. Comput. Chem.* **2003**, *24*, 298 – 309.
[58] S. Fantacci, A. Migani, M. Olivucci, *J. Phys. Chem. A* **2004**, *108*, 1208 – 1213.
[59] B. Paizs, E. Tajkhorshid, S. Suhai, *J. Phys. Chem. B* **1999**, *103*, 5388 – 5395.
[60] E. Tajkhorshid, B. Paizs, S. Suhai, *J. Phys. Chem. B* **1999**, *103*, 4518 – 4527.
[61] M. Sugihara, V. Buss, P. Entel, J. Hafner, A. N. Bondar, M. Elstner, T. Frauenheim, *Phase Transitions* **2004**, *77*, 31 – 45.
[62] G. Steinberg, M. Ottolenghi, M. Sheves, *Biophys. J.* **1993**, *64*, 1499 – 1502.
[63] M. Caravetta, X. Zhao, O. G. Johannessen, W. Cheu Lai, M. A. Verhoeven, P. H. M. Bovee-Geurts, P. J. E. Verdegem, S. Kiihne, H. Luthman, H. J. M. de Groot, W. J. de Grip, J. Lugtenburg, M. H. Levitt, *J. Am. Chem. Soc.* **2004**, *126*, 3948 – 3953.
[64] S. W. Lin, G. G. Kochendoerfer, K. S. Carroll, D. Wang, R. A. Mathies, T. P. Sakmar, *J. Biol. Chem.* **1998**, *273*, 24583 – 24591.
[65] V. Buss, *Chirality* **2001**, *13*, 13 – 23.
[66] V. Buss, M. Sugihara, P. Entel, J. Hafner, *Angew. Chem.* **2003**, *115*, 3365 – 3367; *Angew. Chem. Int. Ed.* **2003**, *42*, 3245 – 3247.
[67] M. Wanko, M. Hoffmann, P. Strodel, A. Koslowski, W. Thiel, F. Neese, T. Frauenheim, M. Elstner, *J. Phys. Chem. B* **2005**, *109*, 3606 – 3615.

Received: January 31, 2005
Revised: June 13, 2005

